

# Quantum Teleportation from a Propagating Photon to a Solid-State Spin Qubit

W. B. Gao, P. Fallahi, E. Togan, A. Delteil, Y. S. Chin, J. Miguel-Sanchez, and A. Imamoglu

*Institute of Quantum Electronics, ETH Zurich, CH-8093 Zurich, Switzerland.*

The realization of a quantum interface between a propagating photon used for transmission of quantum information, and a stationary qubit used for storage and manipulation, has long been an outstanding goal in quantum information science [1]. A method for implementing such an interface between dissimilar qubits is quantum teleportation [2–4], which has attracted considerable interest not only as a versatile quantum-state-transfer method but also as a quantum computational primitive [5, 6]. Here, we experimentally demonstrate transfer of quantum information carried by a photonic qubit to a quantum dot spin qubit using quantum teleportation. In our experiment, a single photon in a superposition state of two colors – a photonic qubit – is generated using selective resonant excitation of a neutral quantum dot. We achieve an unprecedented degree of indistinguishability of single photons from different quantum dots by using local electric and magnetic field control. To teleport a photonic qubit, we generate an entangled spin-photon state [7–9] in a second quantum dot located 5 meters away from the first and interfere the photons from the two dots in a Hong-Ou-Mandel set-up. A coincidence detection at the output of the interferometer heralds successful teleportation, which we verify by measuring the resulting spin state after its coherence time is prolonged by an optical spin-echo pulse sequence. The demonstration of successful inter-conversion of photonic and semiconductor spin qubits constitute a major step towards the realization of on-chip quantum networks based on semiconductor nano-structures [10].

Semiconductor quantum dots (QD) have been at the forefront of two seemingly uncorrelated approaches to experimental quantum information science [1]: on the one hand, single QDs in photonic nanostructures have been used to realize high-efficiency sources for single-photons [11–13] with potential applications in quantum key distribution [14] and linear optics quantum computation [6]. On the other hand, single spins confined in quantum dots have been extensively studied as promising solid-state qubits with long coherence time and a potential for integration on a chip

[15–20]. By realizing teleportation of the quantum state of a single photon in a superposition of two frequency components generated by one QD to the spin-state of another QD located in a different cryostat, we demonstrate that these two auspicious features of QDs can be combined to realize an elementary process relevant for a quantum network [10].

The key step in photon-to-spin quantum teleportation protocol [2] is the two-photon interference of the photon (in mode A) to be teleported with a second photon (in mode B) that is initially in a maximally entangled state with the target spin state (Fig. 1). Detection of a coincidence event at the output of a Hong-Ou-Mandel (HOM) interferometer heralds the successful teleportation of the quantum state of the single photon in mode A, given by the arbitrary superposition of its two frequency components,  $|\psi_p\rangle = \alpha|\omega_b\rangle_A + \beta|\omega_r\rangle_A$ , to the QD electron spin-state, which after the completion of the protocol reads  $|\psi_e\rangle = \alpha|\downarrow\rangle + \beta|\uparrow\rangle$ .

To generate a photonic qubit, we use a neutral self-assembled InGaAs QD (QD1 or QD3) where the elementary optical excitations from the unique ground state  $|0\rangle$  are the two fundamental exciton states  $X_r$  and  $X_b$  that are split in energy by the anisotropic electron-hole exchange interaction. The exciton state  $X_r$  ( $X_b$ ) decays at rate  $\Gamma_1$  by spontaneous emission of a photon at frequency  $\omega_r$  ( $\omega_b$ ) back into  $|0\rangle$  (Fig. 2a). A laser field with a pulse duration short compared to  $\Gamma_1^{-1}$  and resonant with either of these two exciton states results in the generation of a single-color single photon pulse. Alternatively, applying a two-color laser pulse that is simultaneously resonant with both  $X_r$  and  $X_b$  results in the generation of a single-photon that is in a superposition of the two central frequency components  $\omega_r$  and  $\omega_b$ . The left-hand side of Figure 1 shows the experimental set-up we use to generate such a single-photon qubit. An amplitude electro-optic modulator (EOM) is used to generate 400ps pulses from a continuous-wave (cw) laser field. A second EOM is used to generate sidebands that enable us to resonantly drive  $X_r$  and  $X_b$  simultaneously (Supplementary Information). The generated pulse is depicted in Figure 2a: the beats at  $\omega_b - \omega_r$  demonstrate that the single-photon is in a coherent superposition of two frequencies. Photon correlation measurements carried out on the emitted light in turn show strong antibunching, proving that our scheme generates a nearly ideal single-photon pulse (Fig. 2a inset).

A high teleportation fidelity requires a high degree of indistinguishability of the two photons generated by two QDs placed in separate cryostats. To determine the degree of indistinguishability we attain, we use single photons generated by two neutral QDs, QD1 and QD2, each tuned using external electric and magnetic fields to ensure that their transition frequencies  $\omega_r$  and  $\omega_b$  are

identical. Figure 2b shows the time resolved coincidences between the two output ports of the HOM interferometer as a function of the time delay between the photon detection times, when the two photonic qubits generated with either identical or orthogonal polarizations are sent to the input ports of the interferometer. Our measurements reveal that the visibility is  $V = (C_{\perp} - C_{\parallel})/C_{\perp} = 80.2 \pm 2.9\%$ , where  $C_{\parallel}$  ( $C_{\perp}$ ) denotes the integrated number of counts in  $[-1.2 \text{ ns}, 1.2 \text{ ns}]$  time window when the photon polarizations in the input ports are identical (orthogonal). This represents the highest value reported to date for photons generated by two different QDs (see Sec. C of the Supplementary Information) [21, 22]. Introducing a half period time-delay for one of the single-photon pulses also renders the photonic qubits distinguishable (Fig. 2b).

To generate an entangled spin-photon pair, we use the trion emission from the single-electron charged state of QD2 [7–9], driven using a combination of resonant excitation and non-resonant rotation pulses as depicted in the right hand side of Fig. 1. The photonic qubit that is coupled to the mode A is generated by the neutral QD3, which is in the same cryostat as QD1 and whose exciton transition energy is nearly identical to that of the QD2 trion. Figure 2c shows the relevant energy-level diagram as well as the allowed optical transitions for QD2 in Voigt geometry where an external magnetic field  $B_x = 0.7\text{T}$  is applied perpendicular to the growth direction. To ensure that  $\omega_b - \omega_r$  of QD3 matches the electron Zeeman energy of QD2, a separate magnetic field of 0.12 T is applied to QD3. Moreover, the electric fields applied separately to the QD2 and QD3 are adjusted such that their emission frequencies ( $\omega_b$  and  $\omega_r$ ) are identical. The ground states of the QD are identified by the orientation of the electron spin, with  $|\uparrow\rangle$  ( $|\downarrow\rangle$ ) denoting spin parallel (anti-parallel) to the magnetic field direction. Spontaneous emission of H (V) polarized photon at frequency  $\omega_r$  ( $\omega_b$ ) from the trion state  $|T_r\rangle$  at rate  $\Gamma_2/2$  brings the QD back into the  $|\downarrow\rangle$  ( $|\uparrow\rangle$ ) state, resulting in the maximally entangled state [7]

$$|\Psi\rangle = \frac{1}{\sqrt{2}}(|\downarrow\rangle|\omega_r; H\rangle_B + i|\uparrow\rangle|\omega_b; V\rangle_B) \quad . \quad (1)$$

After erasing the polarization information using a polarizer transmitting  $H - iV$  polarized light, the spin-photon entangled state reads  $|\Psi\rangle = \frac{1}{\sqrt{2}}(|\downarrow\rangle|\omega_r\rangle_B - |\uparrow\rangle|\omega_b\rangle_B)$  [7]. Here, we indicated that the photon that is entangled with the spin is channeled into the photonic mode B, which constitutes the second input mode of the HOM interferometer (Fig. 1).

Hyperfine interaction between the electron spin and the QD nuclei leads to a spin-decoherence time of  $T_2^* \sim 1\text{ns}$ . To ensure that the electron spin coherence is intact when the coincidence de-

tection in the HOM interferometer heralds successful teleportation in  $\sim 11\text{ns}$  after the generation of the entangled spin-photon state, we introduce a spin-echo scheme that extends the coherence of the electron spin [23]. For an echo time  $T_{echo} = 13\text{ns}$ , measurement of the spin-photon correlations in the rotated basis demonstrates that spin-photon entanglement fidelity is  $F > 0.63 \pm 0.02$  (Fig. 2c); this lower bound for the fidelity is determined predominantly by the detection jitter ( $60\text{ps}$ ) (Supplementary Information). We emphasize that despite the similarity with the single-photon pulse-shape in Fig. 2a, what is depicted in Fig. 2c is the time dependence of the coincidence counts as a function of generation time of the entangled spin-photon pair, with  $t = 0$  denoting the rise-time of the entanglement generation pulse (see the pulse sequence depicted in Fig. 2c).

The state of the coupled system consisting of two photons in modes A & B and the QD spin prior to the beam splitter is

$$|\Psi\rangle = (\alpha|\omega_b\rangle_A + \beta|\omega_r\rangle_A) \otimes \frac{1}{\sqrt{2}}(|\omega_r\rangle_B|\downarrow\rangle - |\omega_b\rangle_B|\uparrow\rangle) \quad (2)$$

If the photons in modes A & B are indistinguishable in every aspect but their internal (color) state, the only possibility for a simultaneous coincidence detection at the output of the HOM interferometer is to have the input two-photon state in  $|\varphi_S\rangle = \frac{1}{\sqrt{2}}(|\omega_b\rangle_A|\omega_r\rangle_B - |\omega_r\rangle_A|\omega_b\rangle_B)$  [24]. Therefore, detection of a coincidence projects the input photonic state (in modes A&B) to  $|\varphi_S\rangle$  [2]. The spin-state corresponding to this measurement outcome is  $\langle\varphi_S|\Psi\rangle = \alpha|\uparrow\rangle + \beta|\downarrow\rangle$ , as can be verified from Eq. 2. Experimental verification of teleportation is based on three-fold coincidence detection of photons at the the two output modes of the HOM interferometer, together with a photon detection during the spin-measurement/preparation cycle. To verify heralded quantum teleportation, we focus on photons emitted in an  $800\text{ps}$  long time-interval (as depicted in Figs. 3a), which is slightly longer than the QD lifetime ( $650\text{ps}$ ).

In order to demonstrate classical correlations between the color of the photon to be teleported and the final spin state, we use an input photon that is prepared either in  $|\omega_r\rangle_A$  or  $|\omega_b\rangle_A$ . For a mode A photon in  $|\omega_r\rangle_A$ , a three-fold coincidence projects the photon in mode B onto  $|\omega_b\rangle_B$  and the spin onto  $|\uparrow\rangle$ . Figure 3b shows that the same-period (*period 0*) 3-fold coincidences corresponding to a spin measurement in  $|\uparrow\rangle$  are a factor  $\sim 4$  larger than those corresponding to  $|\downarrow\rangle$ . By using an input photon in state  $|\omega_b\rangle_A$ , the *period 0* 3-fold coincidences show that detecting the spin in  $|\downarrow\rangle$  is now  $\sim 4.0$  more likely than detecting it in  $|\uparrow\rangle$  (Fig. 3c), in accordance with the predictions of the teleportation protocol. From these measurements, we obtain the teleported state fidelities

$0.79 \pm 0.1$  ( $0.82 \pm 0.09$ ) for  $|\omega_r\rangle_A$  ( $|\omega_b\rangle_A$ ). We note that the time-resolved three-fold coincidence counts for the input state  $|\omega_b\rangle_A$  (Fig. 3d) show oscillations at  $\omega_b - \omega_r = 4.9\text{GHz}$ .

Demonstration of quantum teleportation requires that coherences in the photonic superposition state at the input mode A are faithfully transferred onto the spin state. To verify this, we prepare the single-photon in mode A in either  $|\omega_r\rangle_A + |\omega_b\rangle_A$  or  $|\omega_r\rangle_A - |\omega_b\rangle_A$ . Since the propagation time of the photons onto the superconducting single-photon detectors (SSPD) is about 11ns, we introduce a spin-echo pulse sequence to ensure that the spin measurement is carried out only after the coincidence detection at the output of the HOM interferometer. The 3-fold coincidences now indicate an enhanced probability for detection of the spin in state  $|\uparrow\rangle + |\downarrow\rangle$  for an input photon in  $|\omega_r\rangle_A + |\omega_b\rangle_A$  and  $|\uparrow\rangle - |\downarrow\rangle$  for an input photon in  $|\omega_r\rangle_A - |\omega_b\rangle_A$  (Figs. 3e,f,g). From these measurements, we obtain the teleported state fidelities  $0.76 \pm 0.03$  ( $0.75 \pm 0.03$ ) for  $|\omega_r\rangle_A + |\omega_b\rangle_A$  ( $|\omega_r\rangle_A - |\omega_b\rangle_A$ ). The overall teleportation fidelity for the above 4 different input photonic states is  $F_T = 0.78 \pm 0.03$ , which is above the classical threshold of  $2/3$  by 3.7 standard deviations.

The measured teleportation fidelity is limited by the small mismatch between the temporal pulse-shapes and the spatial overlap profiles of the two interfering photons, as well as the finite spin-photon entanglement fidelity. We emphasize that, unlike measurements of entanglement fidelity [7–9], the experimentally determined teleportation fidelity is independent of the detector jitter. Prolongation of the spin-echo time in our experiments is limited by dynamical nuclear spin polarization effects [23, 25] that are omnipresent in self-assembled QDs (Supplementary Information).

We expect quantum teleportation from a propagating photonic qubit to a stationary solid-state spin qubit to play a central role in quantum networks where nodes incorporating a small number of spin-qubits are interconnected using photons. While the finite efficiency of quantum state transfer is a limitation in general, the heralding of successful transfer renders the implemented protocol relevant for schemes such as linear optics quantum computation which rely on post-selection on measurement results and where quantum memory for the photons is crucial. Since our photonic qubit is generated by a neutral QD exciton, our experiment can also be considered as the realization of teleportation from the exciton qubit of one QD to the spin qubit of another QD. A natural extension of the quantum teleportation protocol is to replace the photonic qubit with a photon that is entangled with another QD spin; coincidence detection at the output of the HOM interferometer in this case will herald successful generation of a maximally entangled state of two distant spins

that have never directly interacted with each other [26, 27]. Further interesting extensions include quantum teleportation to a decoherence-avoiding singlet-triplet qubit in a QD molecule [28], to a hole-spin [29], or a subsequent transfer of the spin state from the self-assembled QD to a gate-defined QD, where longer coherence times on the order of  $200\mu\text{s}$  and coherent two-qubit gates have been demonstrated [30].

- 
- [1] DiVincenzo, D. P. The physical implementation of quantum computation. *Fortschritte der Physik* **48**, 771-783 (2000).
- [2] Bouwmeester, D. *et al.* Experimental quantum teleportation. *Nature* **390**, 575-579 (1997).
- [3] Sherson, J. F. *et al.* Quantum teleportation between light and matter. *Nature* **443**, 557-560 (2006).
- [4] Chen, Yu-Ao. *et al.* Memory-built-in quantum teleportation with photonic and atomic qubits. *Nature Physics* **4**, 103-107 (2008).
- [5] Gottesman, D. & Chuang, I. L. Demonstrating the viability of universal quantum computation using teleportation and single-qubit operations. *Nature* **402**, 390-393 (1999).
- [6] Knill, E., Laflamme, R. & Milburn, G. J. A scheme for efficient quantum computation with linear optics. *Nature* **409**, 46-52 (2001).
- [7] Gao, W. B., Fallahi, P., Togan, E., Miguel-Sanchez, J. & Imamoglu, A. Observation of entanglement between a quantum dot spin and a single photon. *Nature* **491**, 426-430 (2012).
- [8] De Greve, K. *et al.* Quantum-dot spin-photon entanglement via frequency downconversion to telecom wavelength. *Nature* **491**, 421-425 (2012).
- [9] Schaibley, J. R. *et al.* Demonstration of quantum entanglement between a single electron spin confined to an InAs quantum dot and a photon. *Phys. Rev. Lett.* **110**, 167401 (2013).
- [10] Cirac, J. I., Zoller, P., Kimble, H. J., & Mabuchi, H. Quantum State Transfer and Entanglement Distribution among Distant Nodes in a Quantum Network. *Phys. Rev. Lett* **78**, 3221-3224 (1997).
- [11] Michler, P. *et al.* A quantum dot single-photon turnstile device. *Science* **22**, 2282-2285 (2000).
- [12] Santori, C., Fattal, D., Vučković, J., Solomon, G. S. & Yamamoto, Y. Indistinguishable photons from a single-photon device. *Nature* **419**, 594-597 (2002).
- [13] Claudon, J. *et al.* A highly efficient single-photon source based on a quantum dot in a photonic nanowire. *Nature Photonics* **4**, 174-177 (2010).
- [14] Bennett, C. H. & Brassard, G. Quantum cryptography: public key distribution and coin tossing. Proc. IEEE Int. Conference on Computers, Systems and Signal Processing, Bangalore, India, *IEEE Press, New York*, **175** (1984).
- [15] Loss, D. & DiVincenzo, D. P. Quantum computation with quantum dots. *Phys. Rev. A* **57**, 120-126

- (1998).
- [16] Imamoğlu, A. *et al.* Quantum information processing using quantum dot spins and cavity QED. *Phys. Rev. Lett.* **83**, 4204-4207 (1999).
  - [17] Kroutvar, M. *et al.* Optically programmable electron spin memory using semiconductor quantum dots. *Nature* **432**, 81-84 (2004).
  - [18] Petta, J. R. *et al.* Coherent manipulation of coupled electron spins in semiconductor quantum dots. *Science* **309**, 2180-2184 (2005).
  - [19] Press, D., Ladd, T. D., Zhang, B. & Yamamoto, Y. Complete quantum control of a single quantum dot spin using ultrafast optical pulses. *Nature* **456**, 218-221 (2008).
  - [20] A. Greilich *et al.* Ultrafast optical rotations of electron spins in quantum dots. *Nature Physics* **5**, 262-266 (2009).
  - [21] Flagg, E. B. *et al.* Interference of single photons from two separate semiconductor quantum dots. *Phys. Rev. Lett.* **104**, 137401 (2010).
  - [22] Patel, R. B. *et al.* Two-photon interference of the emission from electrically tunable remote quantum dots. *Nature Photonics* **4**, 632-635 (2010).
  - [23] D. Press *et al.* Ultrafast optical spin echo in a single quantum dot. *Nature Photonics* **4**, 367-370 (2010).
  - [24] Olmschenk, A. *et al.* Quantum teleportation between distant matter qubits. *Science* **323**, 486-489 (2009).
  - [25] Urbaszek, B. *et al.* Nuclear spin physics in quantum dots: An optical investigation. *Rev. Mod. Phys.* **85**, 79-133 (2013).
  - [26] Moehring, D. L. *et al.* Entanglement of single-atom quantum bits at a distance. *Nature* **449**, 68 (2007).
  - [27] Bernien, H. *et al.* Heralded entanglement between solid-state qubits separated by three metres. *Nature* **497**, 86-90 (2013).
  - [28] Weiss, K. M., Elzerman, J. M., Delley, Y. L., Miguel-Sanchez, J. & Imamoğlu, A. Coherent two-electron spin qubits in an optically active pair of coupled InGaAs quantum dots. *Phys. Rev. Lett.* **109**, 107401 (2012).
  - [29] Brunner, D. *et al.* A coherent single-hole spin in a semiconductor. *Science* **325**, 70-72 (2009).
  - [30] Bluhm, H. *et al.* Dephasing time of GaAs electron-spin qubits coupled to a nuclear bath exceeding 200  $\mu$ s. *Nature Physics* **7**, 109-113 (2010).

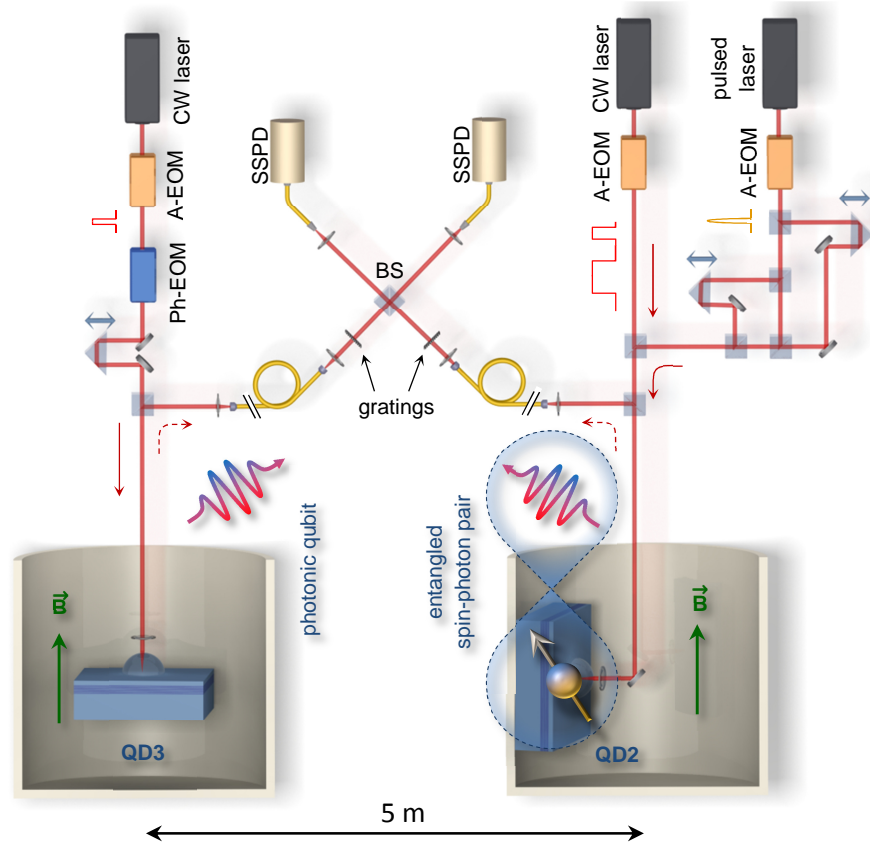
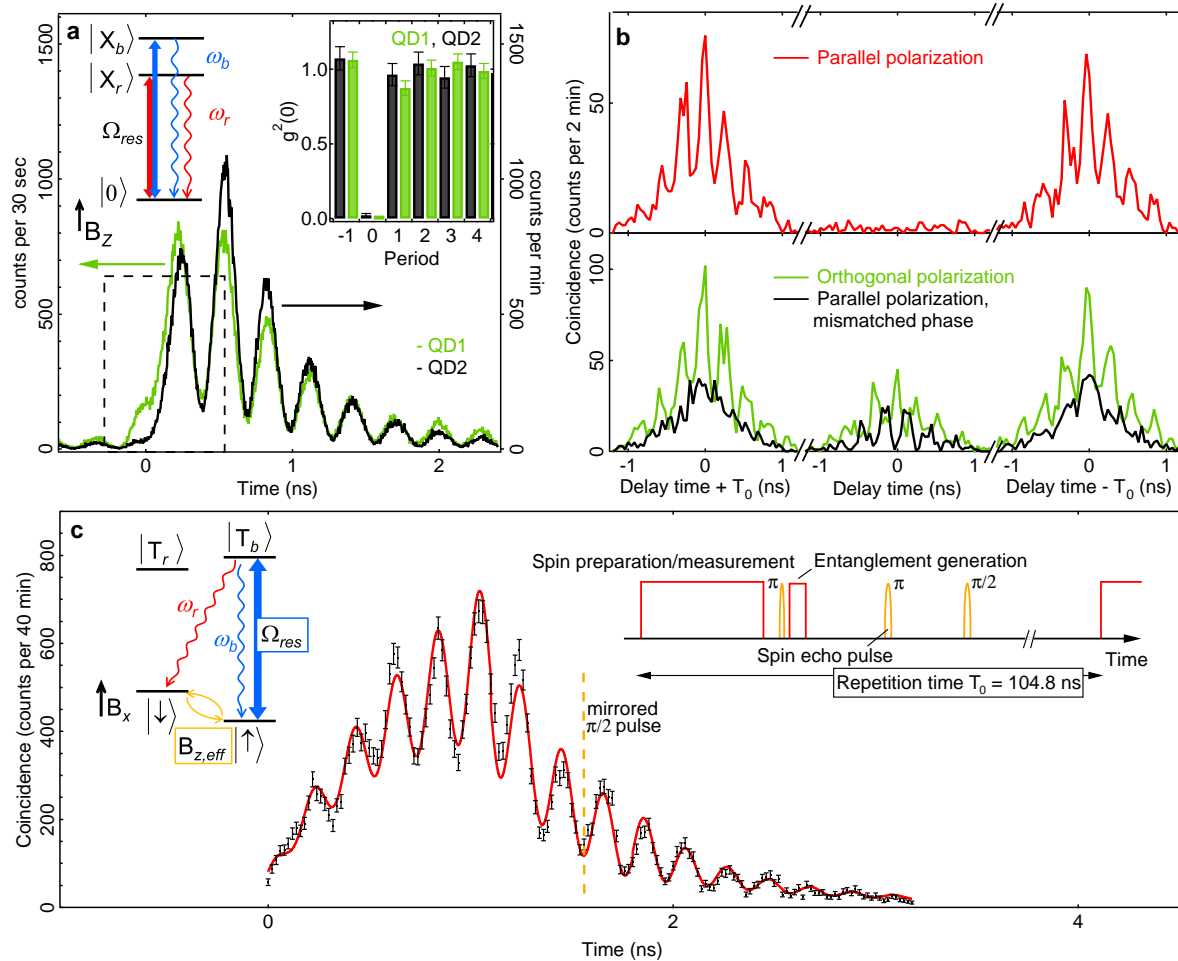
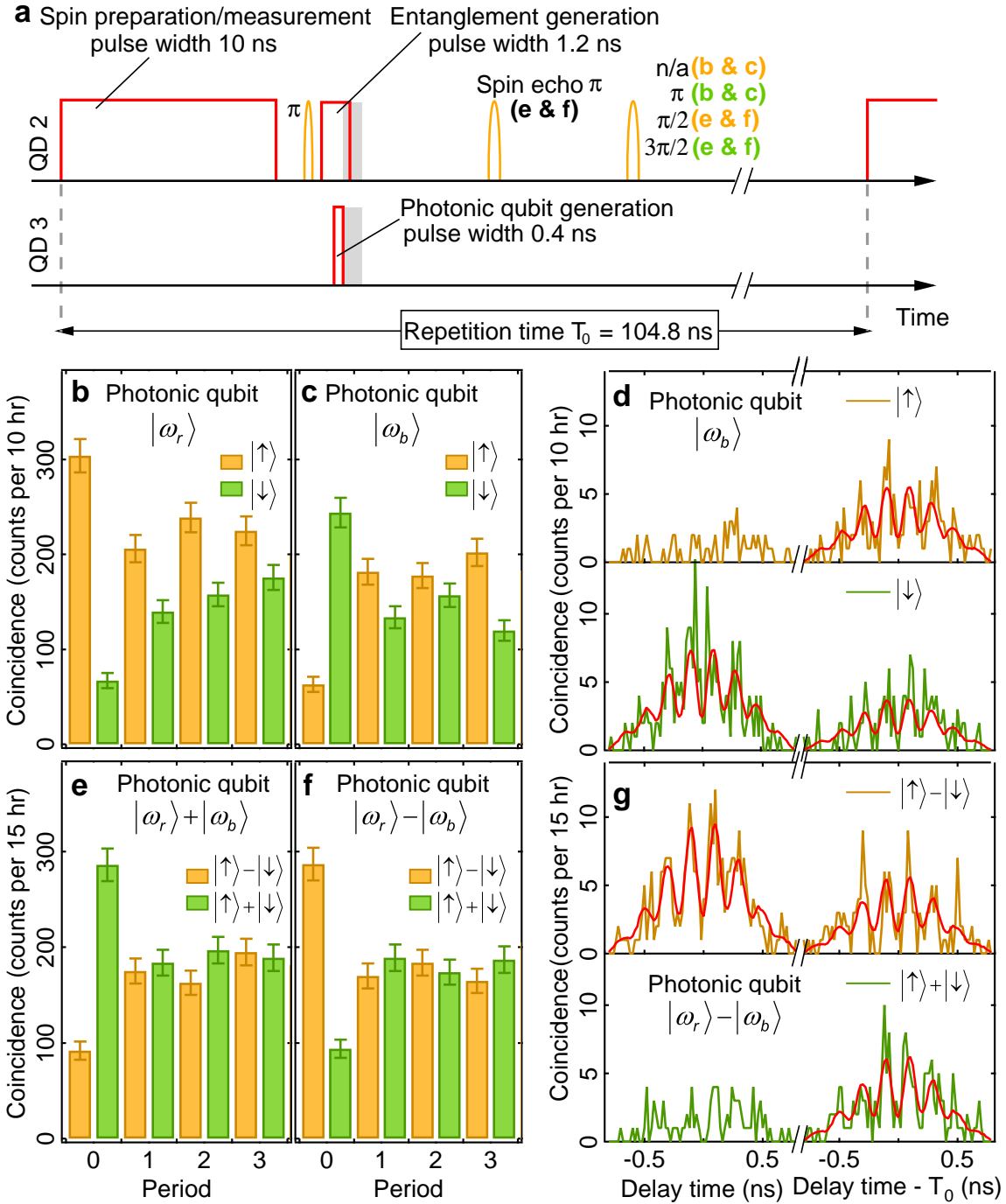


Figure 1: The neutral exciton transitions in a single InGaAs quantum dot (QD3) are resonantly excited by a  $0.4ns$  laser pulse. Upon spontaneous emission the QD generates a photon in an experimentally tunable superposition state of the two neutral exciton transition frequencies, forming a single photon qubit. A different quantum dot (QD2) in the single-electron charged state, under a perpendicular external magnetic field, is resonantly excited by a sequence of pulses that initialize the electron spin and excite the blue negatively charged exciton (trion). An entangled spin-photon pair is generated upon spontaneous emission from the trion state. The two QDs are located in separate liquid Helium bath cryostats that are  $\sim 5m$  apart. The emitted single photons from the two QDs are collected into single mode fibers and sent to interfere on a beam splitter in a Hong-Ou-Mandel setup. In both arms, transmission gratings with  $70GHz$  bandwidth are used to filter out the  $200GHz$  detuned  $4ps$  rotation laser as well as the phonon sideband emission from the QDs. Superconducting single photon detectors (SSPD) are used to detect the photons on the output arms of the beam splitter. A coincidence detection on the two SSPDs heralds a successful teleportation of the state of the photonic qubit to that of the electron spin in QD2, which is measured by the same two SSPDs at a later time.



**Fig.2: Characterization of the photonic qubit, photon indistinguishability and entanglement generation.** (a) Time resolved resonance fluorescence counts are plotted for QD1 (green) and QD2 (black). A  $0.8ns$  two color laser pulse (dashed line) that is resonant with both excitonic transitions  $|X_b\rangle$  and  $|X_r\rangle$  excites the QD (upper left panel); subsequent spontaneous emission generates a single photon in a superposition of  $\omega_b$  and  $\omega_r$ . The matched oscillations of the emission from the two QDs at  $\Delta = \omega_b - \omega_r = 3.45GHz$  indicate that the generated photonic qubit states are nearly identical. The upper right panel shows photon correlation ( $g^2$ ) measurements on the two QDs using the emitted photons detected after the excitation pulse is turned off, indicating that the likelihood of two or more photon detection events is very small. (b) The photonic qubits depicted in a are incident on a beam splitter. Coincidence counts on the two output arms of the beam splitter are plotted as a function of the delay between the recorded photon arrival times.  $T_0$  is the pulse repetition time of  $13.1ns$ . As the photons are indistinguishable when the input modes have parallel polarization (top panel), the coincidence counts within the time window  $[-1.2 ns, 1.2 ns]$  are 11 times smaller than those in which the second photon is detected in other periods. In the bottom panel, the photons are rendered distinguishable either through their polarization (green) or their phase (black), leading to a center peak coincidence count that is 2 times smaller than the other periods. (c) QD2 is prepared in the single-electron charged state. An external magnetic field of  $B_x = 0.7T$  is applied in the Voigt geometry leading to the energy-level diagram depicted in the left panel. The pulse sequence used for the generation of spin-photon entangled state and measurement of correlations after a spin-echo sequence is shown in the upper right panel. The center panel shows the photons emitted during and after the entanglement generation pulse, conditioned upon a spin measurement in the  $\frac{1}{\sqrt{2}}(|\uparrow\rangle - |\downarrow\rangle)$  state. The oscillations in the depicted coincidence counts at  $\Delta = \omega_b - \omega_r = 4.9GHz$  are due to the beating between the two frequency components of the projected photonic superposition state.



**Fig. 3: Demonstration of quantum teleportation.** (a) The teleportation pulse sequence applied to QD2 for entanglement generation and spin measurement, as well as to QD3 for photonic qubit generation (see Fig. 2 for details). (b, c) Classical correlations between the state of the photonic qubit and the state of the electron spin: the plots show 3-fold coincidence counts between the two output arms of the beam splitter during the  $0.8ns$  time interval depicted by the grey box in a and a photon detection during the following spin measurement pulse ( $period = 0$ ) or during a later pulse period ( $period > 0$ ). An enhanced probability for the spin state  $|\uparrow\rangle$  ( $|\downarrow\rangle$ ) as well as a decreased probability for  $|\downarrow\rangle$  ( $|\uparrow\rangle$ ) is observed when the photonic qubit was initially prepared in  $|\omega_r\rangle$  ( $|\omega_b\rangle$ ). The coincidence counts, measured for  $period > 0$ , differ for measurement of the spin in  $|\uparrow\rangle$  and  $|\downarrow\rangle$  states, due to the fact that the unconditioned  $|\uparrow\rangle$  population is  $> 0.5$ ; this is a consequence of excitation probability to the  $|T_b\rangle$  state during the entanglement generation pulse being  $< 1$ . (d) Time resolved 3-fold coincidence counts corresponding to the data plotted in the first two periods in c. Red lines are guides to the eye, showing the expected oscillations for coincidences. (e, f) Quantum correlations between the state of the photonic qubit, prepared either in  $|\omega_r\rangle + |\omega_b\rangle$  e or  $|\omega_r\rangle - |\omega_b\rangle$  f, and the spin qubit. The 3-fold coincidence counts are measured as described above. A spin echo  $\pi$ -pulse is applied to prolong the spin coherence time. Detection of a coincidence on the beam splitter in e (f) projects the spin into  $|\uparrow\rangle + |\downarrow\rangle$  ( $|\uparrow\rangle - |\downarrow\rangle$ ), as evidenced by the observed correlations. (g) Time resolved coincidence counts corresponding to the data plotted for the first two periods in f. Red lines are guides to the eye.